Fibroblast growth factor 2 contributes to the effect of salidroside on dendritic and synaptic plasticity after cerebral ischemia/reperfusion injury

Sisi Li[1,2], Yechen Lu[1,2], Daofang Ding[2], Zhenzhen Ma[1,2], Xiangxin Xing[1,2], Xuyun Hua[2,4], Jianguang Xu[1,2,3]

[1]School of Rehabilitation Science, Shanghai University of Traditional Chinese Medicine, Shanghai 201203, PR China
[2]Department of Rehabilitation Medicine, Yueyang Hospital of Integrated Traditional Chinese and Western Medicine, Shanghai University of Traditional Chinese Medicine, Shanghai 200437, PR China
[3]Department of Hand Surgery, Huashan Hospital, Fudan University, Shanghai 200040, PR China
[4]Department of Trauma and Orthopedics, Yueyang Hospital of Integrated Traditional Chinese and Western Medicine, Shanghai University of Traditional Chinese Medicine, Shanghai 200437, PR China

Correspondence to: Jianguang Xu; **email:** jianguangxu@fudan.edu.cn

ABSTRACT

Ischemic stroke, a serious neurological disease, is associated with cell death, axonal and dendritic plasticity, and other activities. Anti-inflammatory, anti-apoptotic, promote dendritic and synaptic plasticity are critical therapeutic targets after ischemic stroke. Fibroblast growth factor-2 (FGF2), which is involved in the cyclic adenosine monophosphate (cAMP)/protein kinase A (PKA)/CAMP response element (CRE)-binding protein (CREB) pathway, has been shown to facilitate dendritic and synaptic plasticity. Salidroside (Sal) has been reported to have anti-inflammatory, anti-oxidative, and anti-apoptotic effects; however, the underlying mechanisms of Sal in promoting dendritic and synaptic plasticity remain unclear. Here, the anti-inflammatory, anti-apoptotic, dendritic and synaptic plasticity effects of Sal were investigated in vitro in PC12 cells under oxygen-glucose deprivation/reoxygenation (OGD/R) conditions and in vivo in rats with middle cerebral artery occlusion/reperfusion (MCAO/R). We investigated the role of Sal in promoting dendritic and synaptic plasticity in the ischemic penumbra and whether the FGF2-mediated cAMP/PKA/CREB pathway was involved in this process. The present study demonstrated that Sal could significantly inhibit inflammation and apoptosis, and promote dendritic and synaptic plasticity. Overall, our study suggests that Sal is an effective treatment for ischemic stroke that functions via the FGF2-mediated cAMP/PKA/CREB pathway to promote dendritic and synaptic plasticity.

INTRODUCTION

Stroke is currently the second leading cause of death worldwide and can be classified into haemorrhagic and ischemic stroke. Among stroke patients, more than 80% suffer from cerebral ischemia, which is caused by the blockage of an artery supplying blood to the brain [1, 2].

Recent studies have shown that acute ischemic stroke leads to diverse pathophysiological changes, such as brain oedema, neuronal damage and synaptic dysfunction [3]. The behavioural changes and functional recovery after ischemic stroke are closely related to dendrite and synaptic plasticity [4]. Synapses are plastic, a phenomenon that is governed by the temporal

patterns of presynaptic and postsynaptic activity. Postsynaptic activity can be determined by the properties of dendrites, indicating that dendrites play an important role in, and, to a certain extent, dominate synaptic plasticity [5]. While the initial degeneration of dendrites may not lead to the death of many injured neurons, when allowed to continue, dendrites will gradually degenerate, leading to a decrease in synaptic efficiency and, eventually, neuron death [6]. Therefore, available treatment interventions may be able to retard early dendritic degeneration to prevent the death of injured neurons.

First defined by Astrup J, the ischemic penumbra is a region characterized by extremely dynamic biochemical changes in the acute stage of cerebral ischemia that is not yet irreversibly impaired [7]. As an area of metabolically damaged tissue located around the most seriously affected ischemic centre, local cerebral blood flow can be restored by timely therapeutic intervention [8, 9].

It has been suggested that growth factors may be therapeutic targets for ischemic stroke [10]. Fibroblast growth factor-2 (FGF2, also known as bFGF) is a single-chain polypeptide containing 146 amino acids that serves as an important component of the FGF superfamily [11, 12]. The biological activity of FGF2 is mediated by its binding to a high-affinity cell surface receptor, FGF receptor 1 (FGFR1) [13]. FGF2 plays a critical role in cell–cell signaling between neurons during development and is thought to be responsible for neurogenesis, neuroprotection, and synaptic plasticity [14–16]. FGF2 enhances axonal branching and synaptogenesis in neurons and accelerates the bifurcation and growth of axonal branches [17]. FGF2 has been proposed to contribute to the recovery of neurologic function by increasing the dendritic arborization and spine density after ischemic brain injury [18]. By promoting axon spouting and new synapse formation, FGF2 can reduce the infarct size and promote the restoration of sensory motor functions.

FGF2 is involved in the cyclic adenosine monophosphate (cAMP)/protein kinase A (PKA) pathway, and FGF2 can be promoted by PKA to promote cell survival [19]. Studies have demonstrated that cAMP/PKA is involved in synaptic development and plasticity in the cortex [20]. It has been shown that cAMP is associated with synaptic neurotransmitters between motor and sensory neurons [21]. Physiologically, PKA acts as a central transducer in cAMP signaling, playing an essential role in a variety of physiological and developmental processes, such as learning and memory [22], neuron differentiation

regulation, and especially, axonal/dendritic morphogenesis coordination [23]. In addition, the mechanism underlying the effects of cAMP/PKA on ischemia/reperfusion injury is correlated with the regulation of apoptosis [24] and inflammation [25]. CAMP response element (CRE)-binding protein (CREB) is the target of PKA, and the PKA-mediated phosphorylation of CREB at Ser133 is a well-characterized CREB activation mechanism. Interestingly, CREB is also a downstream molecule of FGF2/FGFR1 signaling [26, 27]. Numbers of studies have demonstrated that CREB acts as a transcription factor and plays a key role in promoting cell metabolism, proliferation, survival and remodelling of dendrites and axons [28, 29]. These findings demonstrate that the FGF2-mediated cAMP/PKA/CREB pathway has a neuro-protective effect by modulating the inflammatory response in ischemic brain injury.

Salidroside (Sal, Figure 1A shows the chemical structure of Sal), the major phenylpropanoid glycoside extract from *Rhodiola rosea* L, has diverse pharmacological activities. Many recent reports and reviews have highlighted that Sal may exert anti-inflammatory [30], neuroprotective effects [31] and improve cognitive function [32] both in vitro and in vivo. Previous studies have also indicated that Sal exhibits potential neuroprotective activity by regulating genes related to nerve synaptic plasticity [33, 34].

In the current study, we hypothesized that Sal may alleviate ischemia/reperfusion injury by reducing inflammation, inhibiting apoptosis and promoting dendritic and synaptic plasticity in the ischemic penumbra. Our study also investigated the role of FGF2-mediated cAMP/PKA/CREB pathway participates in the effect of Sal.

RESULTS

Sal upregulates FGF2/FGFR1 under OGD/R conditions in PC12 cells

Western blot, qPCR and immunofluorescence were performed to explore the effects of Sal on FGF2/FGFR1 mRNA and protein expression. The qPCR and western blot results suggested that OGD/R obviously elevated the mRNA and protein expression levels of FGF2/FGFR1, and the expression levels of FGF2/FGFR1 were higher in the Sal-pre-treated groups compared with the OGD/R group (Figure 1C–1G). The results of immunofluorescence staining for FGF2/NeuN were consistent with those of western blot and qPCR (Figure 1B). Those findings suggested that Sal efficiently increased the expression of FGF2/FGFR1.

Sal attenuates OGD/R-induced proinflammatory cytokine secretion

The effect of Sal on neuroinflammation induced by OGD/R was detected based on changes in inflammatory cytokine production. The results showed the protein and mRNA levels of proinflammatory mediators, including tumor necrosis factor alpha (TNF-α), interleukin-1β (IL-1β) and IL-6 were increased after OGD/R, Sal significantly reversed the inflammation induced by OGD/R (Figure 2).

Sal inhibits neuronal apoptosis induced by OGD/R

Immunofluorescence staining of cleaved caspase 3 (c-caspase 3) was performed to determine whether Sal could prevent neuronal apoptosis. As shown in Figure 3A, OGD/R increased neuronal apoptosis while the neurons in the Sal-pre-treated groups exhibited decreased c-caspase 3 staining. In addition, the expression levels of c-caspase 3, B-cell lymphoma-2 (Bcl-2) and Bcl-2-associated X protein (Bax) were analysed by western blot (Figure 3B-3E) and qPCR (Figure 3F–3H), the results showed that the incidence of apoptosis was significantly increased after OGD/R and decreased in Sal-pre-treated groups. The CCK-8 assay results indicated that compared with that in the OGD/R group, the cell viability in the Sal-pre-treatment groups was markedly increased (Figure 3I). These results indicated that Sal treatment significantly inhibited OGD/R-induced neuronal apoptosis.
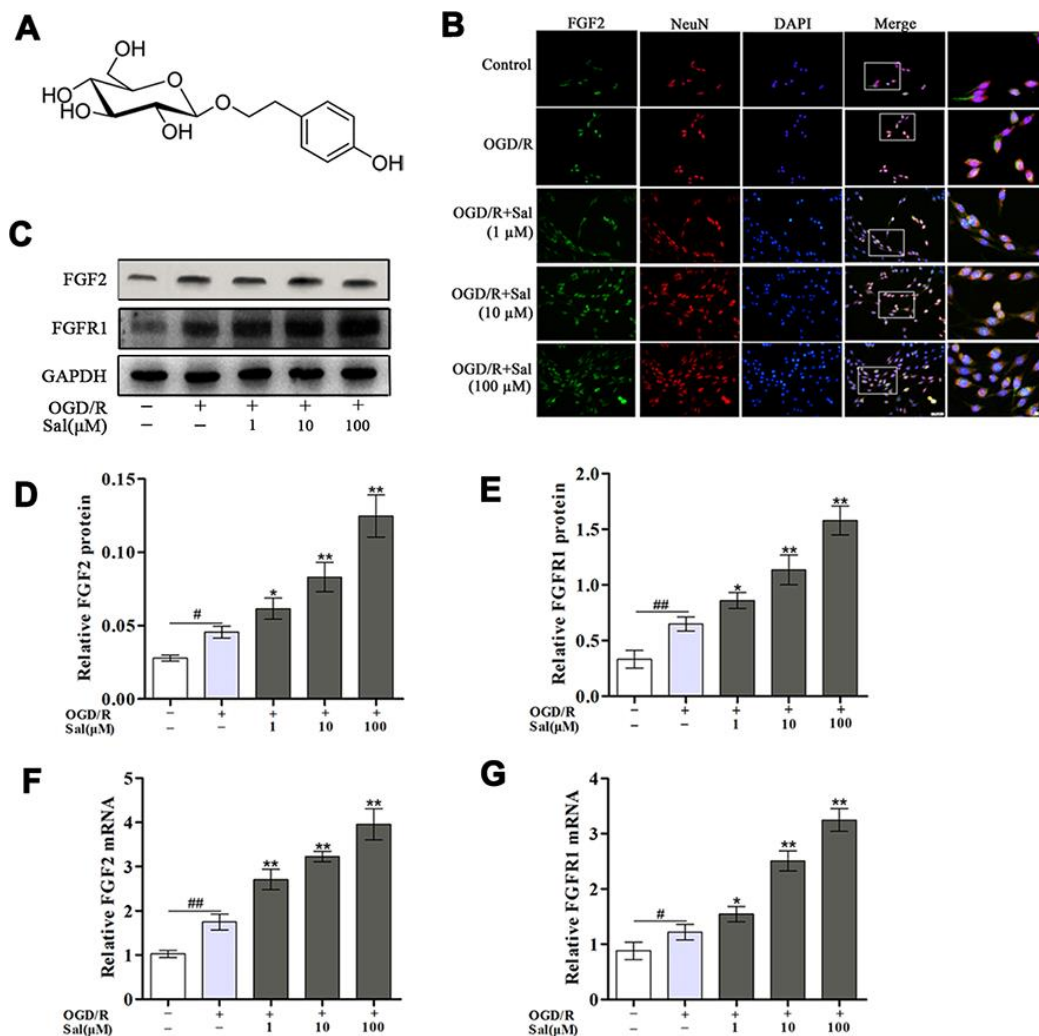

Figure 1. Sal increases FGF2 and FGFR1 expression in PC12 cells after OGD/R. (**A**) The chemical structure of Sal. (**B**) Double staining for FGF2-positive (green) and NeuN-positive (red) neurons (scale bars are 20 μm and 10 μm). (**C**–**E**) Representative western blot bands and protein expression of FGF2 and FGFR1 in PC12 cells. GAPDH was used as a protein loading control and for band density normalization. (**F**, **G**) The mRNA expression levels of FGF2 and FGFR1. Values are expressed as the mean ± SD. #$p < 0.05$, ##$p < 0.01$ vs. control; *$p < 0.05$, **$p < 0.01$ vs. OGD/R.

Sal promotes the production of synaptic-associated proteins after OGD/R

To investigate the effect of Sal on synaptic-associated proteins after OGD/R in PC12 cells, we detected changes in post-synaptic density protein 95 (PSD95), synapsin I and synaptotagmin. Compared with those in the control group, the expression levels of PSD95, synapsin I and synaptotagmin under OGD/R conditions were markedly decreased. Significantly increased level of those were observed in the Sal-pre-treated groups compared to the OGD/R group (Figure 4), suggesting that Sal promoted the growth of synaptic-associated proteins after OGD/R.

Sal reduces the brain infarct volume and neurological deficits in rats with MCAO/R

We investigated the effect of Sal and H-89 (inhibitor of PKA) on infarct size on day 7 after middle cerebral artery occlusion/reperfusion (MCAO/R). Infarct size was decreased after Sal treatment as determined by 2,3,5-triphenyltetrazolium chloride (TTC) staining. The H-89 group had larger infarct volumes than other groups (Figure 5A, 5B). In addition, Sal treatment significantly reduced neurological deficits (Figure 5C). The effects of Sal on neuronal morphology after MCAO/R were determined by haematoxylin-eosin (HE) staining (Figure 5D). The arrangement of brain tissue in the Sal groups was more regular than the untreated group, while brain tissue damage in the H-89 group was more severe than that in the other groups. In the H-89

group, brain tissue was irregularly arranged and unevenly stained, the intercellular space was increased, the number of cells was significantly decreased and the nuclei were small or absent. Nissl staining showed that the Sal groups had less neuronal apoptosis or necrosis than the MCAO/R group (Figure 5E). Furthermore, treatment with Sal resulted in a significant decrease in the number of apoptotic cells in comparison with that in the MCAO/R group, as identified by TUNEL staining, while the H-89 group exhibited increased apoptotic cell numbers compared with the MCAO/R group (Figure 5F).

Sal upregulates the FGF2-mediated cAMP/PKA/CREB signaling pathway in MCAO/R rats

We evaluated the expression of cAMP, PKA, CREB, p-CREB, FGF2 and FGFR1 in the ischemic penumbra by western blot and qPCR, revealing that the expression levels of cAMP, PKA, p-CREB, FGF2 and FGFR1 were markedly increased in the MCAO/R group compared with the sham group. The expression levels of FGF2 and FGFR1 were significantly increased after Sal treatment but were significantly decreased in the H-89 group compared with the MCAO/R group. There was no significant difference in cAMP expression between the MCAO/R and other groups (Figure 6A-6G). According to qPCR analysis, the mRNA expression levels of PKA, p-CREB, FGF2 and FGFR1 were significantly different between the MCAO/R and Sal groups (Figure 6H-6K). We also performed double-immunofluorescence staining for FGF2 and NeuN. As
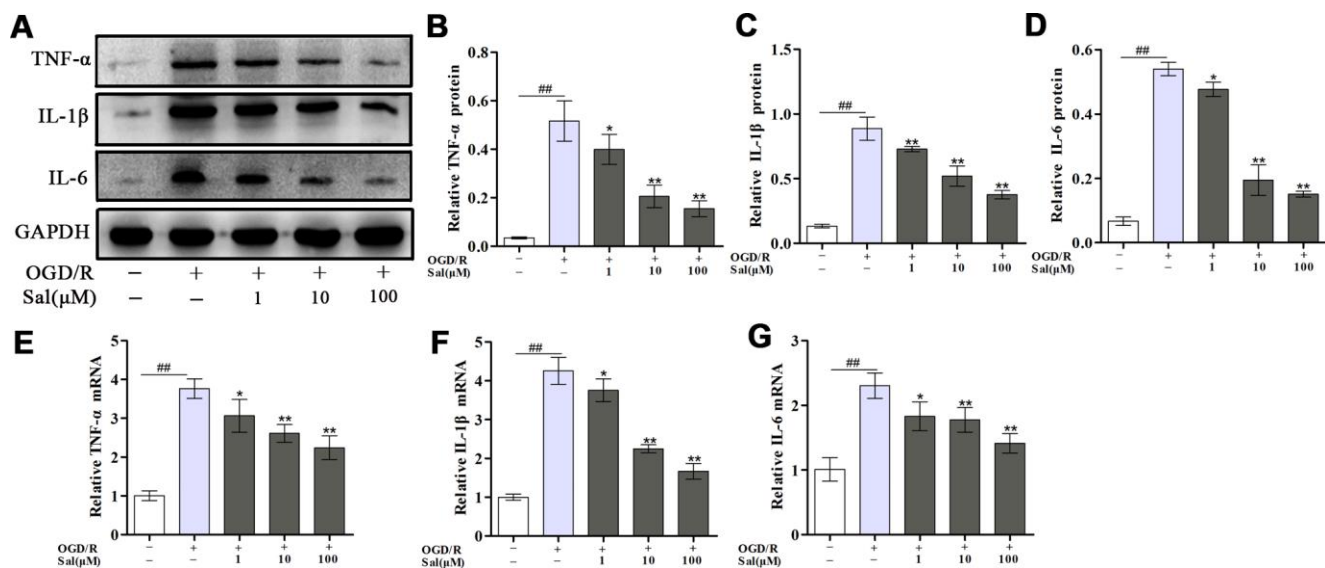

Figure 2. Sal inhibits OGD/R-induced proinflammatory cytokine secretion. (**A–D**) Optical density analysis of the TNF-α, IL-1β and IL-6 proteins. (**E–G**) The mRNA expression levels of TNF-α, IL-1β and IL-6. Values are expressed as the mean ± SD. #$p < 0.05$, ##$p < 0.01$ vs. control; *$p < 0.05$, **$p < 0.01$ vs. OGD/R.

shown in Figure 6L, FGF2 was increased in the MCAO/R group compared with that in the same region in the sham group, while FGF2 in the Sal groups was expressed at substantially higher levels than that in the MCAO/R group.

Sal treatment attenuates proinflammatory cytokine release after MCAO/R

The effect of Sal on neuroinflammation induced by MCAO/R was detected through changes in pro-inflammatory cytokine production. The data showed that the proinflammatory cytokines TNF-α, IL-1β and IL-6 were significantly elevated in the MCAO/R group, treatment with Sal significantly suppressed the amount of TNF-α, IL-1β and IL-6 (Figure 7).

Treatment with Sal inhibits MCAO/R-induced neuron apoptosis

To assess whether Sal prevents neuronal apoptosis, we analysed c-caspase 3, Bcl-2 and Bax levels by western
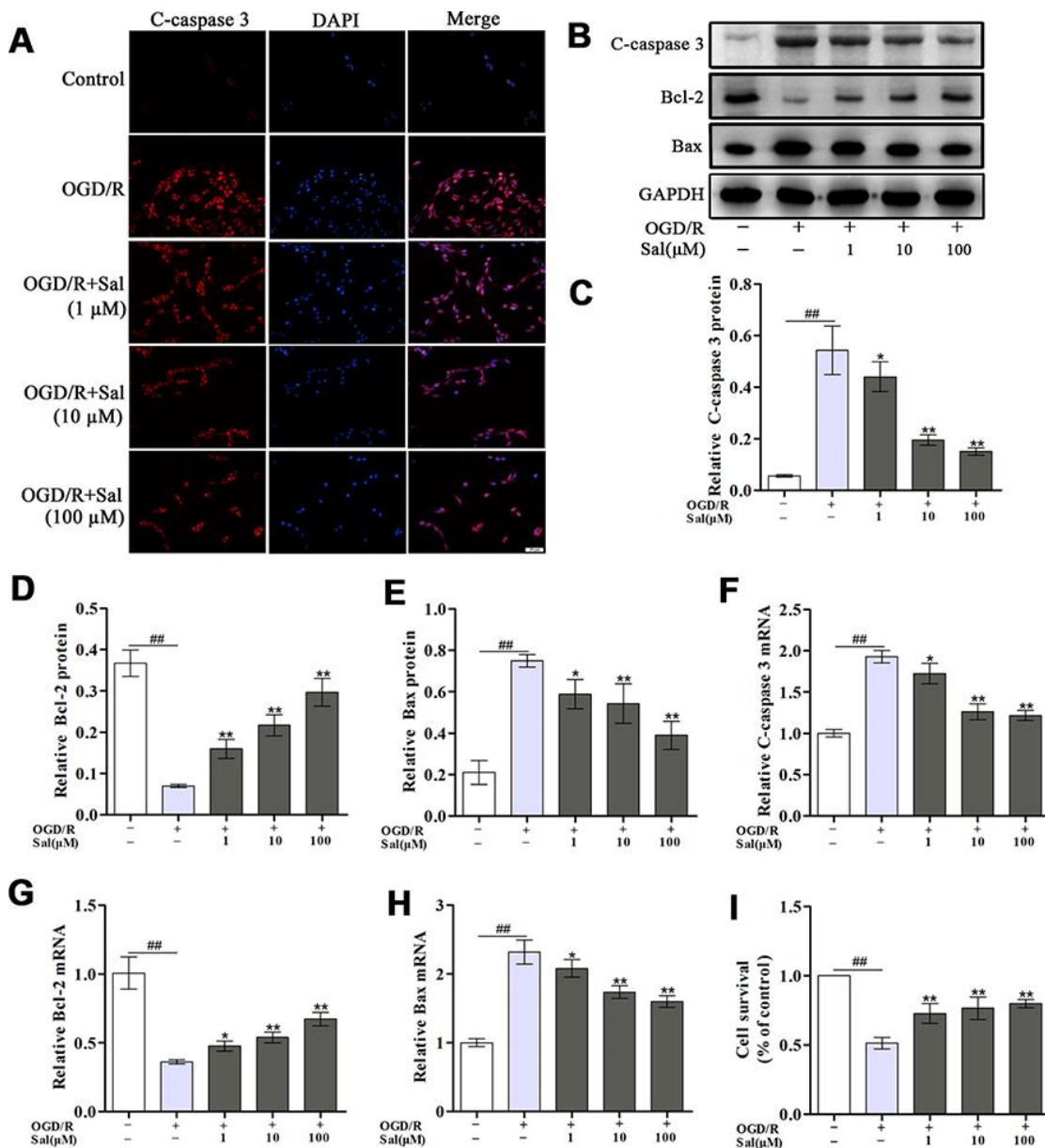

Figure 3. Sal prevents OGD/R-induced neuronal apoptosis. (**A**) Immunofluorescence staining of c-caspase 3 (the scale bar is 20 μm). (**B**–**E**) Representative western blot bands and protein expression of c-caspase 3, Bcl-2 and Bax in each group. (**F**–**H**) QPCR data showing the mRNA expression levels of c-caspase 3, Bcl-2 and Bax. (**I**) The CCK-8 assay was performed to assess cell proliferation. Values are expressed as the mean ± SD. #$p < 0.05$, ##$p < 0.01$ vs. control; *$p < 0.05$, **$p < 0.01$ vs. OGD/R.

blot (Figure 8B-8E) and qPCR (Figure 8F-8H). Our results indicated that Sal treatment exhibited decreased neuronal apoptosis compared with MCAO/R group. Neuronal apoptosis in the H-89 group was significantly worse than that in the MCAO/R group. We also performed immunofluorescence staining for c-caspase 3, the results were consistent with western blot and qPCR analysis (Figure 8A). These results demonstrated that treatment with Sal might be an effective strategy for inhibiting apoptosis and protecting neurons through the FGF2-mediated cAMP/PKA/CREB signaling pathway.

Sal promotes dendritic growth by upregulating the FGF2-mediated cAMP/PKA/CREB signaling pathway

Golgi-Cox staining clearly illustrated a significant decrease in the total number of intersections in both apical and basal dendrites after ischemic reperfusion injury. The number of intersections in apical and basal dendrites were significantly increased in the Sal groups compared with the MCAO/R group (Figure 9I, 9J). Additionally, we detected the total dendritic length, and the numbers of both apical and basal dendritic branches of layer V neurons in the penumbra. The total lengths of

both apical and basal dendrites were significantly decreased after MCAO/R. Compared with the MCAO/R group, the total lengths of both apical and basal dendrites were increased in the Sal groups (Figure 9K, 9L). The total branches of both apical and basal dendrites in the Sal groups were significantly increased compared with those in the MCAO/R group (Figure 9M, 9N). While there were fewer dendrite intersections, fewer dendritic branches and shorter total dendrite length in the H-89 group.

Sal promotes dendritic spine density and synaptic plasticity via upregulation of the FGF2-mediated cAMP/PKA/CREB signaling pathway

To determine whether Sal attenuates dendritic spine damage, we detected changes in dendritic spine density. Both the apical and basal dendritic spine density in the MCAO/R group were markedly decreased compared with the sham group. And both the apical and basal dendritic spine density in the Sal groups were significantly increased compared with the MCAO/R group (Figure 10A–10C). To investigate the role of Sal in synaptic plasticity, we detected changes in synaptic proteins, including PSD95, synapsin I and synaptotagmin. The expression levels of PSD95, synapsin I and synapto-
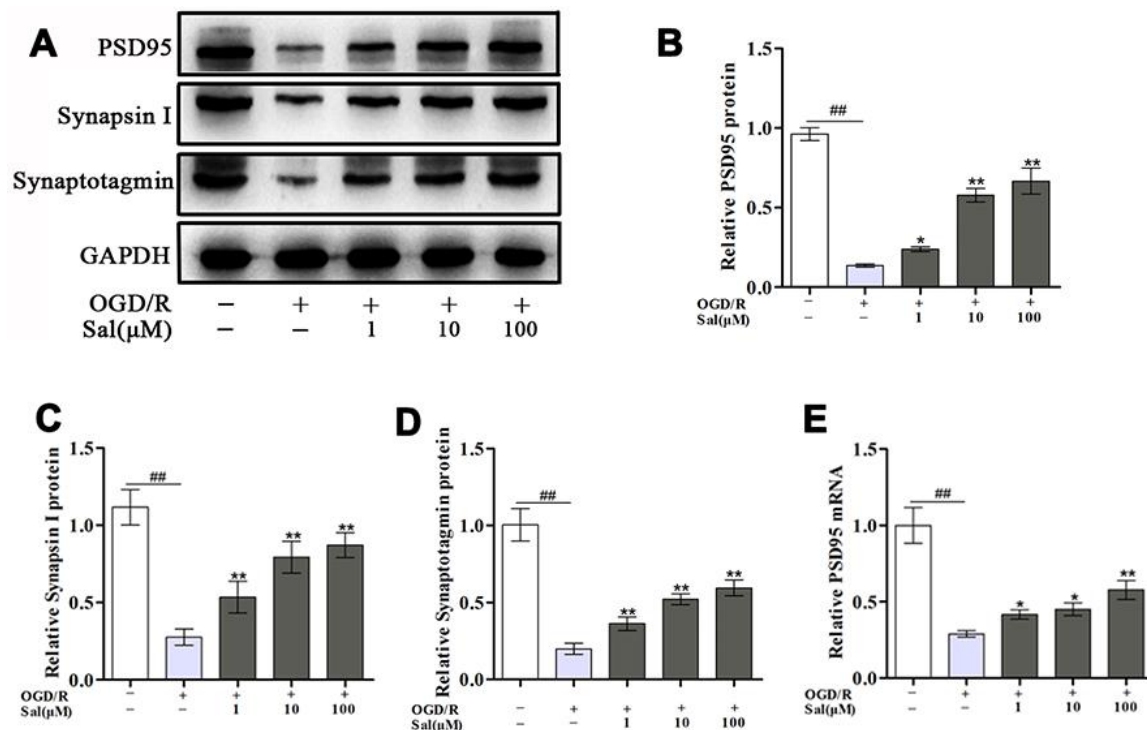

Figure 4. Sal promotes the growth of synaptic-associated proteins after OGD/R. (A–D) Protein expression and quantification analysis of PSD95, synapsin I and synaptotagmin in each group. (E) QPCR data for PSD95. Values are expressed as the mean ± SD. #$p < 0.05$, ##$p < 0.01$ vs. control; *$p < 0.05$, **$p < 0.01$ vs. OGD/R.

tagmin were significantly decreased in the MCAO/R group compared with the sham group. Sal treatment reversed the expression of PSD95, synapsin I and synaptotagmin (Figure 10E-10I), while their expression in the H-89 group was remarkably decreased. The results of immunofluorescence staining for PSD95 were consistent with those of western blot and qPCR (Figure 10D). Furthermore, we examined the effect of Sal on synapse morphology in neurons. The electron microscopy results revealed that the sham group exhibited complete synaptic structures in normal neurons. The MCAO/R group exhibited damaged synaptic structures, and the number of synaptic vesicles was reduced in the ischemic penumbra neurons compared with those in the sham group. A remarkably thickness synaptic membrane, tighter synaptic connections, and more synaptic vesicles were observed in the Sal treatment groups compared with the MCAO/R group. The H-89 group exhibited more significant synapse morphology deficits than the MCAO/R group (Figure 10J).

DISCUSSION

Previous studies have concentrated on the inhibition of neuroinflammation as a potential strategy for the
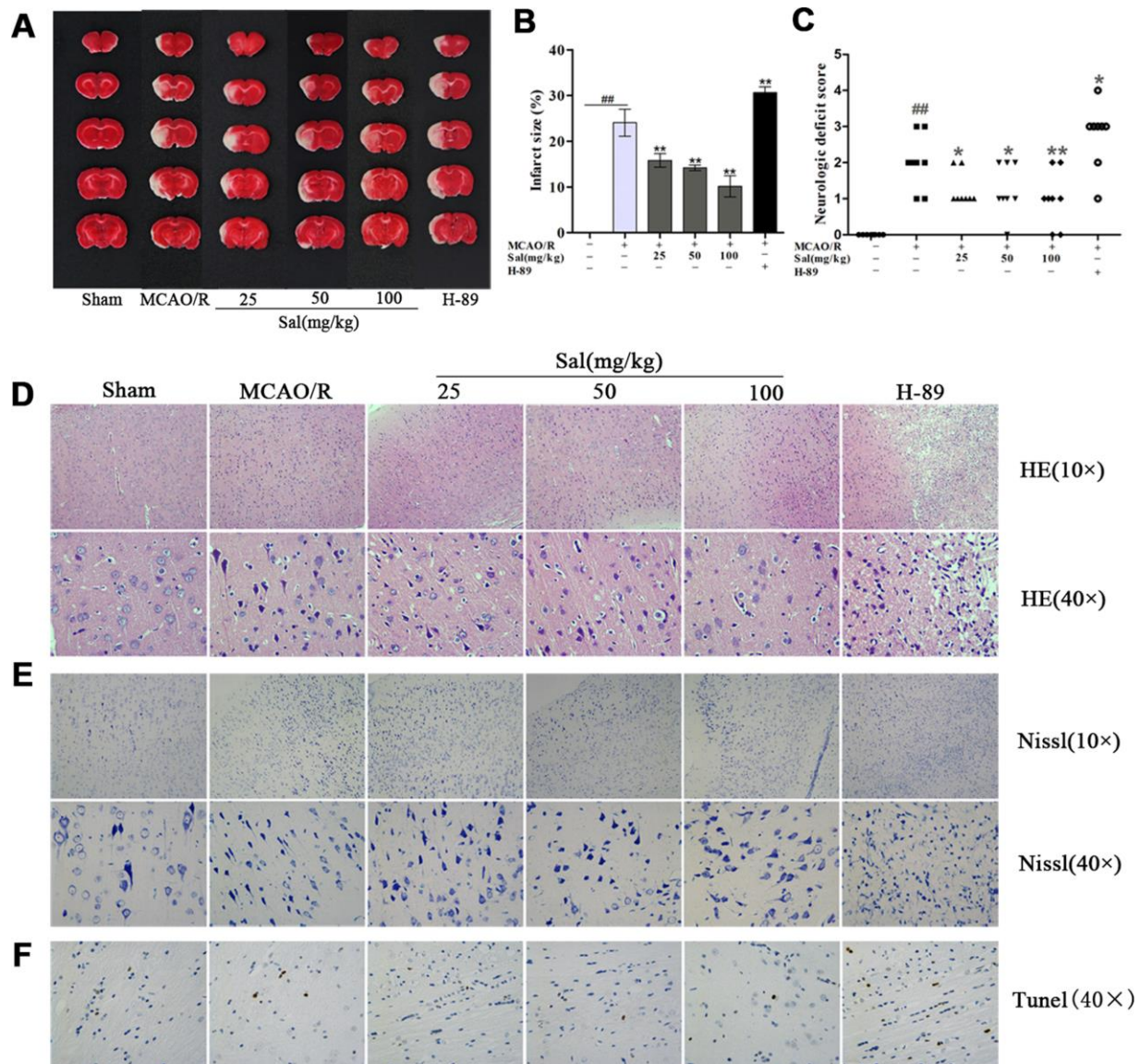

Figure 5. Sal ameliorates tissue structure damage in the ischemic penumbra after MCAO/R. (**A**, **B**) Representative images of ischemic lesions and statistical analysis of infarct volume at 7 days postinjury. (**C**) Neurological deficits. (**D**) HE staining at 7 days after MCAO/R (the scale bars are 100 μm and 20 μm). (**E**) Nissl staining images (the scale bars are 100 μm and 20 μm). (**F**) TUNEL staining in the ischemic penumbra (the scale bar is 20 μm). Values are expressed as the mean ± SD. #$p < 0.05$, ##$p < 0.01$ vs. sham; *$p < 0.05$, **$p < 0.01$ vs. MCAO/R.

treatment of stroke. However, the roles of dendritic modification and synaptic plasticity in neurons and their underlying molecular mechanisms remain unclear. Our results demonstrate that the FGF2-mediated cAMP/PKA/CREB plays a crucial role in dendritic modification and synaptic plasticity. In addition, Sal acts as an effective treatment option through the FGF2-mediated cAMP/PKA/CREB signaling pathway to reduce inflammation, apoptosis and promote dendritic and synaptic plasticity after ischemic stroke.

Ischemic stroke triggers the release of proinflammatory mediators, cell death, axonal damage, and regeneration

inhibition. Anti-inflammation, anti-apoptosis and maintaining the survival of injured neurons is an important process for the protection and regeneration of the nervous system. Cerebral ischemia is followed by an inflammatory reaction, the release of various proinflammatory cytokines, including IL-6, IL-1β and TNF-α, is the main mechanism underlying ischemic inflammatory injury [35, 36]. TNF-α is a potent pro-inflammatory cytokine that exerts pleiotropic functions in ischemic brain injury [37]. IL-1β is a main mediator of inflammation and can induce neuronal apoptosis and promote the production of chemokines [38]. IL-6 plays a comprehensive role in cerebral ischemia and
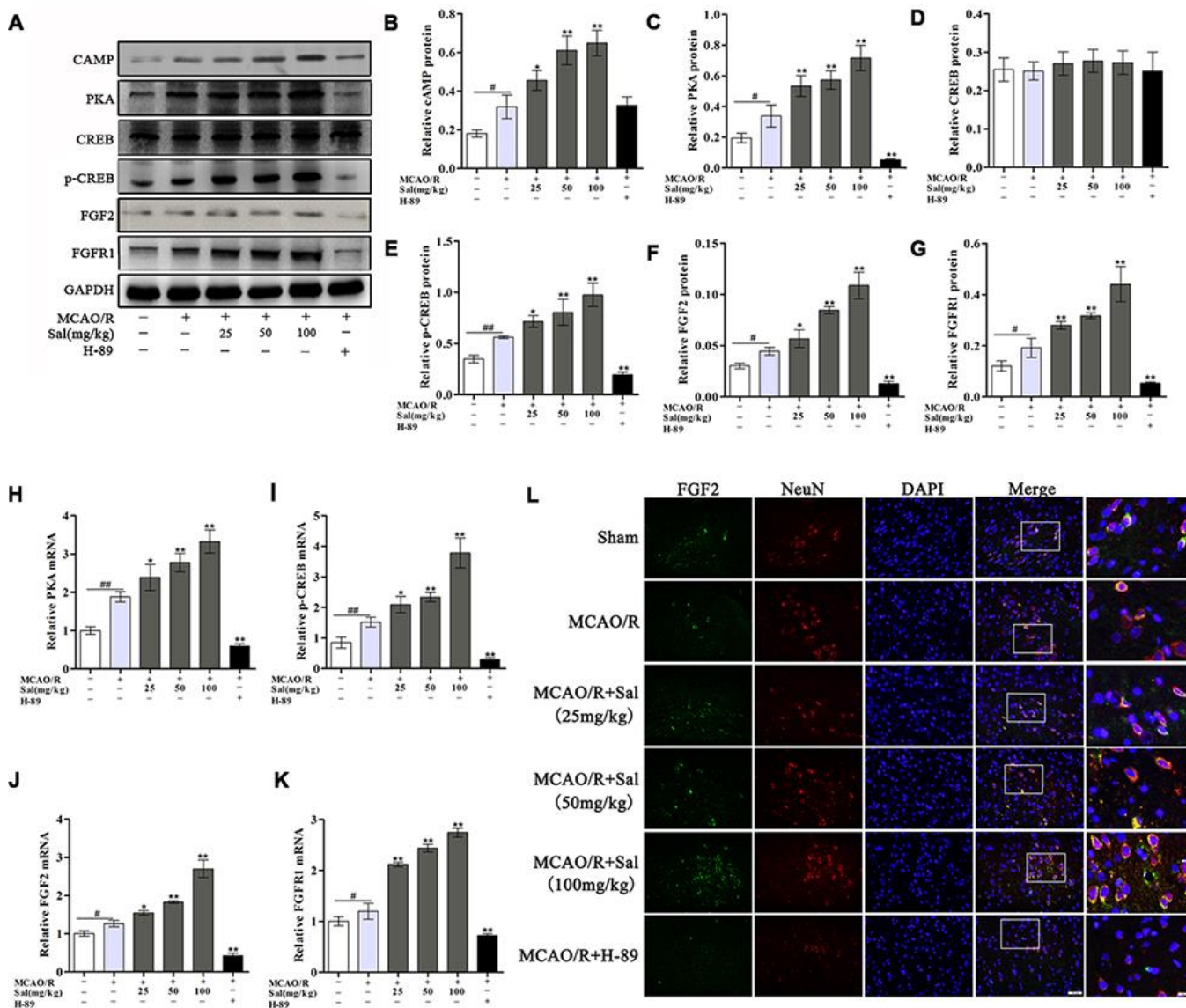

Figure 6. Sal upregulates the FGF2-mediated cAMP/PKA/CREB signaling pathway following MCAO/R. (**A–G**) Representative western blot bands of cAMP, PKA, CREB, p-CREB, FGF2 and FGFR1 in each group. (**H–K**) QPCR analysis of PKA, p-CREB, FGF2 and FGFR1 mRNA expression at 7 days after MCAO/R in different groups. (**I**) Double staining for FGF2-positive (green) and NeuN-positive neurons (red) neurons (the scale bars are 20 μm and 10 μm). Values are expressed as the mean ± SD. #$p < 0.05$, ##$p < 0.01$ vs. sham; *$p < 0.05$, **$p < 0.01$ vs. MCAO/R.
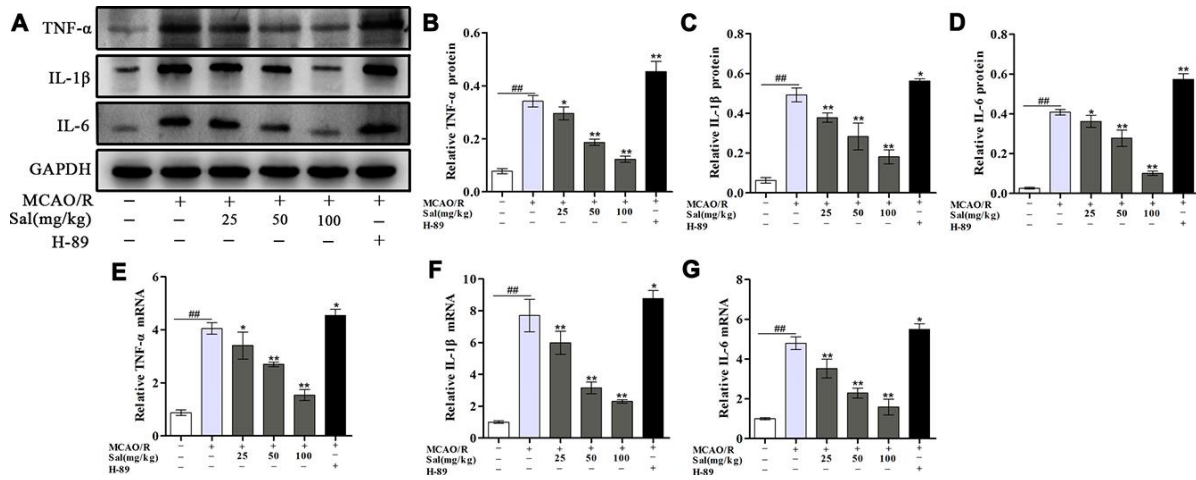
Figure 7. Sal inhibits MCAO/R-induced inflammatory cytokine secretion. (**A–D**) Optical density analysis of the TNF-α, IL-1β and IL-6 proteins. (**E–G**) QPCR results of TNF-α, IL-1β and IL-6 expression. Values are expressed as the mean ± SD. #$p < 0.05$, ##$p < 0.01$ vs. sham; *$p <$ 0.05, **$p < 0.01$ vs. MCAO/R.
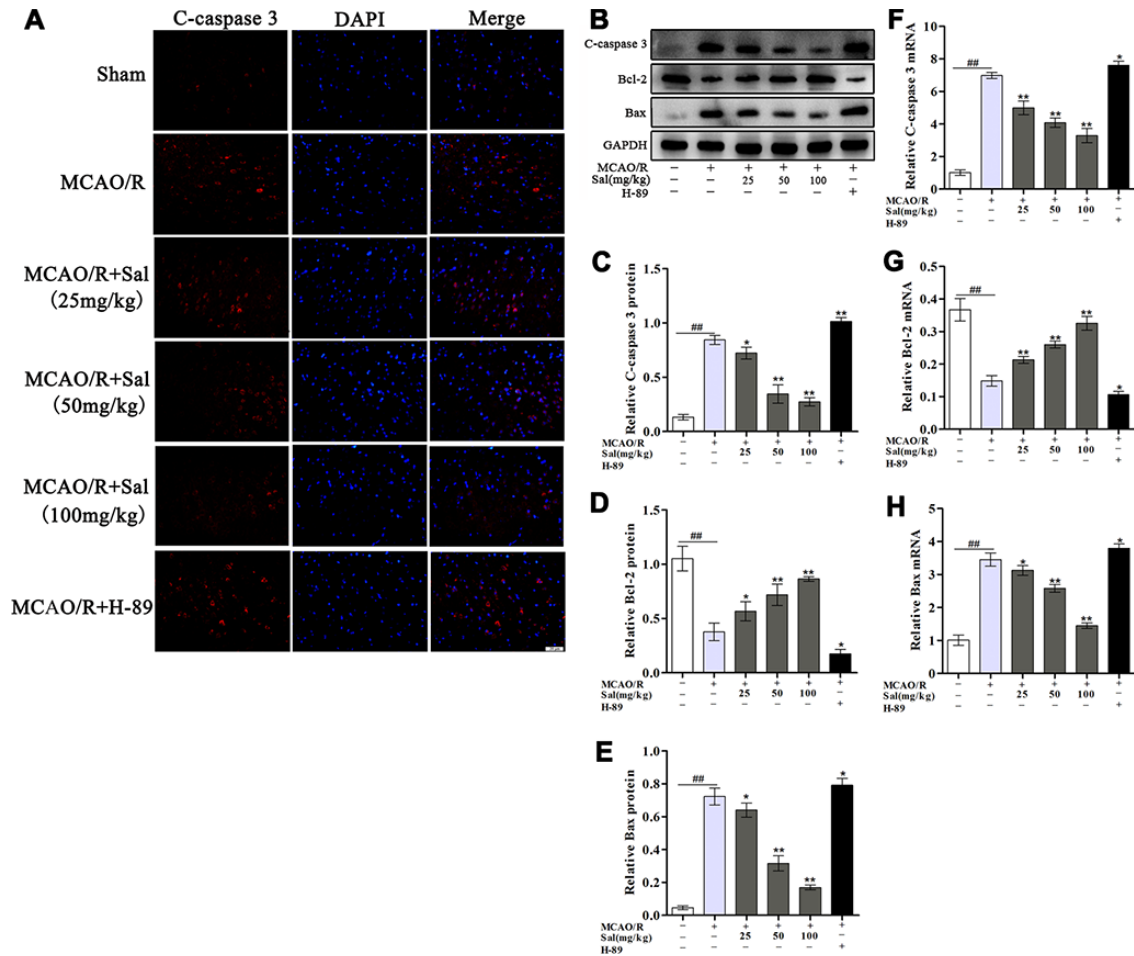

Figure 8. Sal attenuates neuronal apoptosis after MCAO/R. (**A**) Immunofluorescence staining of c-caspase 3 in sections from the ischemic penumbra in each group on day 7 post-MCAO/R (the scale bar is 20 μm). (**B–E**) Protein expression of c-caspase 3, Bcl-2 and Bax from the ischemic penumbra. (**F–H**) QPCR results of c-caspase 3, Bcl-2 and Bax expression. Values are expressed as the mean ± SD. #$p < 0.05$, ##$p <$ 0.01 vs. sham; *$p < 0.05$, **$p < 0.01$ vs. MCAO/R.
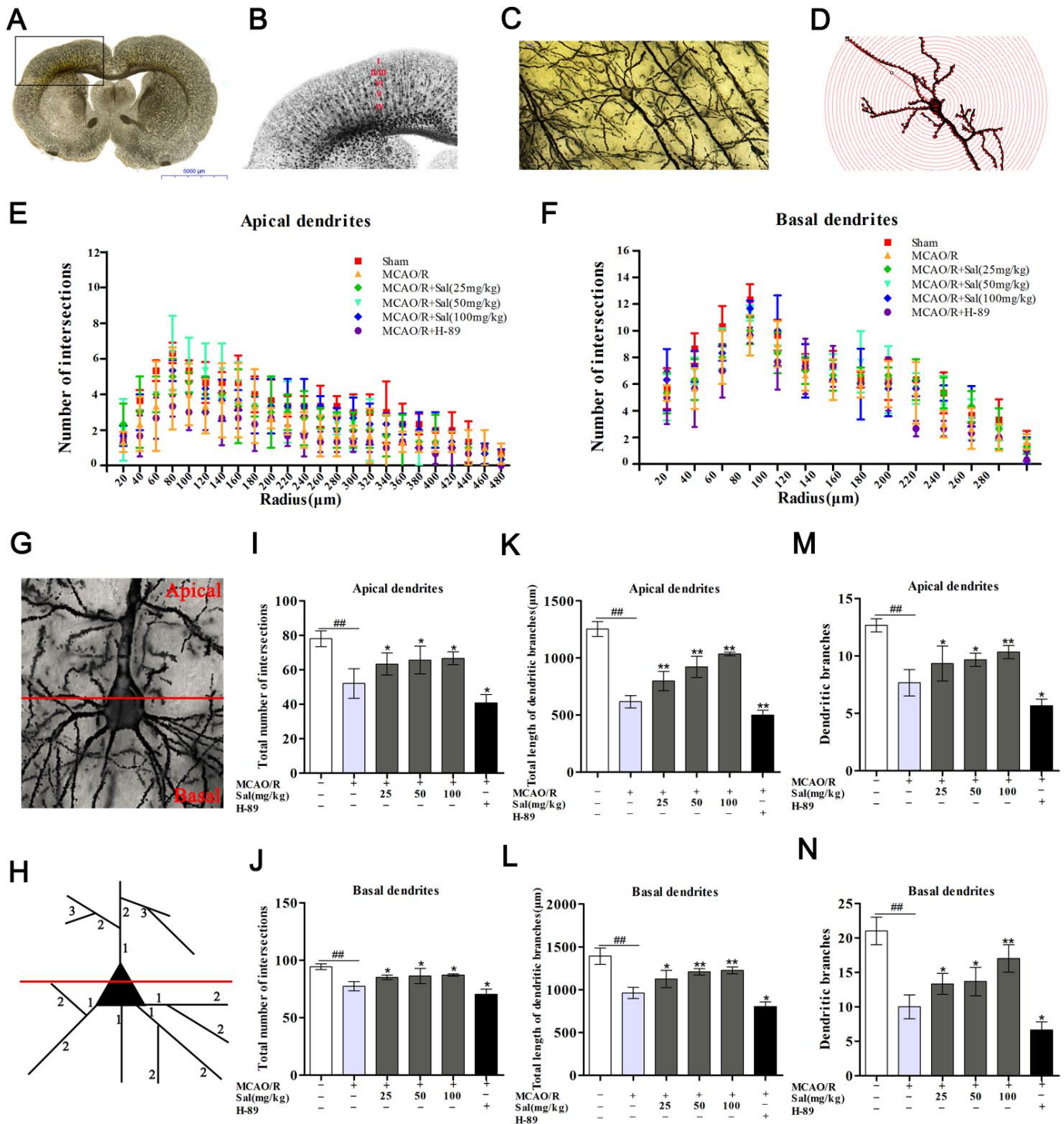
Figure 9. Sal promotes dendritic growth by upregulating the FGF2-mediated cAMP/PKA/CREB signaling pathway. (**A**, **B**) Representative coronal sections processed by Golgi staining methods after MCAO/R. (**C**, **D**) Example of a layer V pyramidal neuron (the scale bar is 20 µm). (**G**) Illustration of the demarcation between the apical (upper) and basal (lower) dendrites. (**H**) Dendritic segments are numbered in the proximal to distal direction from the soma. (**E**, **F**) Distribution of the dendritic intersections at an increasing distance from the soma. (**I**, **J**) Total number of intersections in each group. (**K**, **L**) Total length of dendritic branches. (**M**, **N**) Dendritic branches. Values are expressed as the mean ± SD. #$p < 0.05$, ##$p < 0.01$ vs. sham; *$p < 0.05$, **$p < 0.01$ vs. MCAO/R.
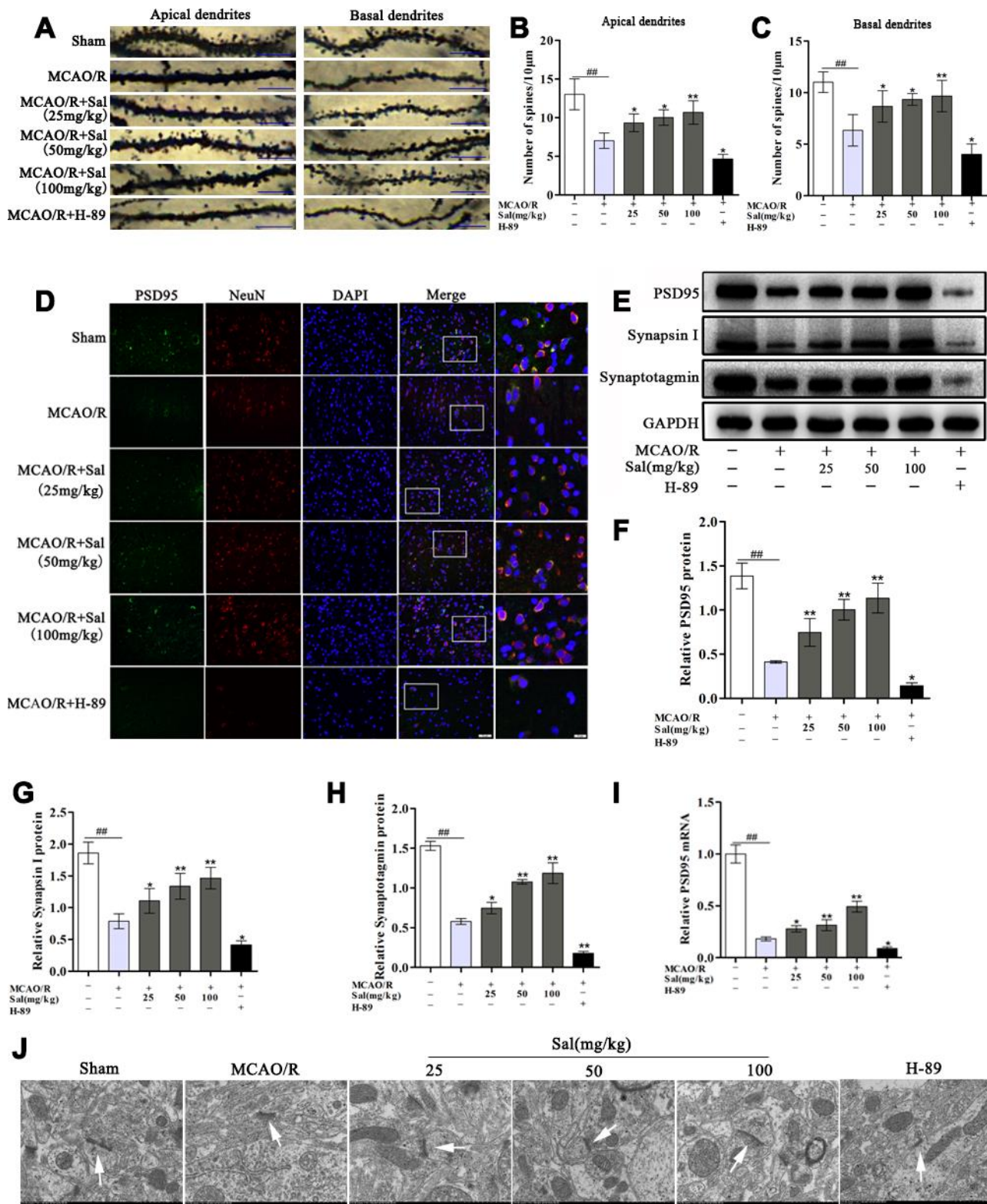
Figure 10. Sal promotes increases in dendritic spine density and synaptic-associated protein expression via upregulating the FGF2-mediated cAMP/PKA/CREB signaling pathway. (**A**) Examples of dendritic spines (the scale bar is 10 μm). (**B**, **C**) Density of dendritic spines. (**D**) Double immunofluorescence staining of PSD95-positive (green) and NeuN-positive (red) neurons from sections in each group on day 7 after MCAO/R (the scale bars are 20 and 10 μm). (**E–H**) Representative western blot bands of PSD95, synapsin I and synaptotagmin in each group. (**I**) QPCR data for PSD95. (**J**) Transmission electron microscopy showed the synaptic structures (the scale bar is 1 μm). Values are expressed as the mean ± SD. #$p < 0.05$, ##$p < 0.01$ vs. sham; *$p < 0.05$, **$p < 0.01$ vs. MCAO/R.

is most prominently identified in neurons of peri-ischemic regions [39]. In the current investigation, Sal was capable of inhibiting inflammation and apoptosis both in vivo and in vitro. It had a significant therapeutic effect on decreasing neurological deficits and alleviating the cerebral infarction volume induced by MCAO/R. And the numbers and morphous of neurons in the ischemic penumbra were better in the Sal treatment groups than in the MCAO/R group.

Synapses are the contact sites between neurons in the central nervous system and therefore contribute to the processing, transfer and storage of information. Dendritic spines are tiny protrusions scattered along the dendrites of many types of neurons and represent the major target of excitatory synapses [40]. Previous studies have shown that a loss of blood supply to the brain, such as a 90% reduction in blood flow, results in dendritic spine loss and irreversible dendritic damage within 10-20 min [41]. In the acute MCAO model, ischemic stroke not only induces neuronal death in the ischemic core area of the infarct but also damages the structure and neurons in the areas surrounding the core (the ischemic penumbra) [42]. The patterns of activity that induce synaptic plasticity at excitatory synapses are disrupted in the zone surrounding the infarct and in areas far from the infarct connected to the infarct area. Spines and dendrites of central neurons represent important sites of synaptic signaling and are the most vulnerable structures after a sudden disruption of blood flow. These changes have been shown to disrupt the neuronal circuitry and impair the function of brain synaptogenesis, and dendritic growth is necessary following cerebral

stroke [43]. The dendrite length represents the total synapse space, and the spine density reflects the density of excitatory synapses to some extent. To increase synaptogenesis, dendritic arborization and increased spine density are potential morphological strategies that enable the brain to reorganize its neuronal circuits.

Recent studies have shown that FGF2 is increased and plays an indispensable role in recovery after ischemic insult [44, 45]. FGF2 is crucial for neurologic recovery by increasing dendritic length and spine density after ischemic brain injury. The FGF2-mediated aberrantly activated cAMP/PKA/CREB pathway is a critical immunological signaling cascade associated with dendritic and synaptic plasticity and thus contributes to recovery after ischemic stroke. The expression of cAMP, PKA and p-CREB was increased at 7 days after ischemic infarction [46, 47]. This pathway can stimulate axon and dendritic sprouting, elongation and branching; increase neurotransmitter release related to synaptic modulation; and strengthen signal transduction in synapses. Synaptotagmin is crucial for the docking of synaptic vesicles and fusion with neuron membrane [48]. Synapsin I, a protein involved in synaptic vesicle formation, synaptogenesis, and regulation of neuro-transmitter release [49]. PSD-95 is a major scaffolding protein in the postsynaptic densities of dendritic spines [50]. A remarkable increase of synaptotagmin, synapsin I and PSD95 expression was revealed indicating the potential function of Sal in synaptogenesis. Golgi staining showed dendrite arbor atrophy and decreased spine density in the MCAO/R group. Compared with the MCAO/R, the H-89 group exhibited a
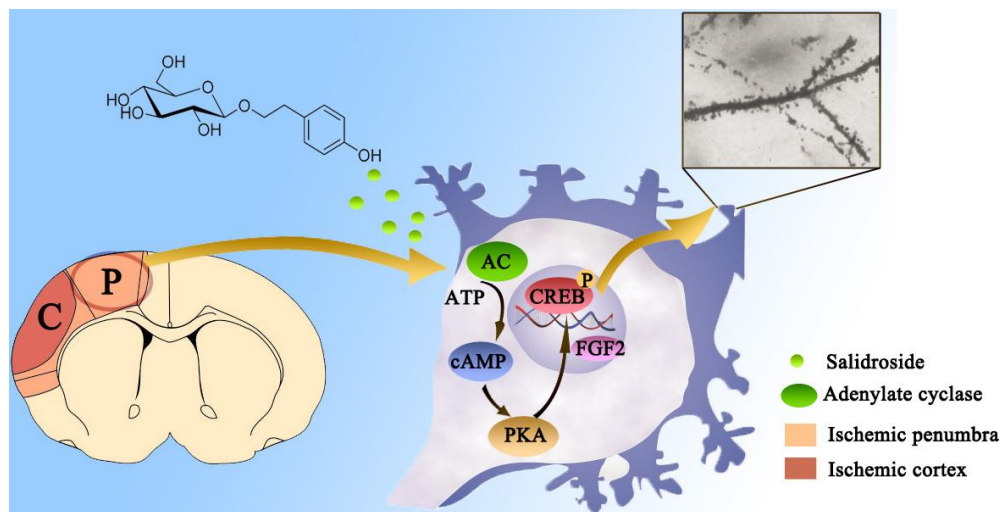

Figure 11. Diagram of the FGF2-mediated cAMP/PKA/CREB signaling pathway contribution to the dendritic and synaptic plasticity of salidroside after focal cerebral ischemia/reperfusion injury.

significantly shorter total dendritic length, decreased dendritic complexity and loss of accompanying neurons. Sal improved the recovery of neurological function by increasing spine formation, dendritic elongation and branching, and the effects of high-dose Sal after stroke were more obvious.

The major limitations of this study should be noted. First, the study aimed mainly to evaluate the effects of Sal on dendritic and synaptic plasticity and the role of FGF2 in these effects. We did not use transgenic knockout or overexpression approaches to elucidate the biological role of FGF2. Second, Long-term potentiation and depression (LTP and LTD) were not used to detect changes at the functional level due to the experimental conditions. Thus, we should improve the experimental design in future studies.

In conclusion, this study indicated that the intervention of Sal reduced inflammation and apoptosis, improved neuronal survival and enhanced dendritic and synaptic plasticity via the FGF2-mediated cAMP/PKA/CREB pathway (Figure 11). Our results demonstrated that Sal may be useful as a therapeutic agent for treating ischemic stroke.

MATERIALS AND METHODS

Reagents and antibodies

Rat adrenal pheochromocytoma cell lines (PC12 cells) were obtained from the Shanghai Institute of Cell Biology (Shanghai, China). Fetal bovine serum (FBS), penicillin/streptomycin, and Dulbecco's modified Eagle's medium (DMEM) were purchased from Gibco Life Technologies (Rockville, MD, US). Cell counting kit-8 (CCK-8) was purchased from Dojindo Laboratories (Tokyo, Japan). The In Situ Cell Death Detection Kit was purchased from Roche Applied Science (Indianapolis, IN, USA). Sal ($C_{14}H_{20}O_7$, CAS#: 10338–51–9, purity > 98%) was purchased from Nanjing Zelang Medical Technological Co. Ltd (Nanjing, China). H-89 dihydrochloride (inhibitor of PKA, HY-15979A) was purchased from Med Chem Express (MCE, New Jersey, USA). Specific antibodies against synapsin I (ab8) and PSD95 (ab18258) were purchased from Abcam (Cambridge Science Park, Cambridge, UK). Specific antibodies against cAMP (DF7741), PKA (AF5450), CREB (AF6188), phosphorylated (p)-CREB (AF3189), FGF2 (DF6038), FGFR1 (AF6156), TNF-α (AF7014), IL-1β (AF5103), IL-6 (DF6087), c-caspase 3 (BF0711), Bcl-2 (AF6139), Bax (AF0120), synaptotagmin (AF6224) and NeuN (DF6145) were obtained from Affinity Biosciences (Cincinnati, OH, USA). Another NeuN antibody (MAB377) was purchased from Millipore (Billerica, MA, USA).

Cell culture and oxygen-glucose deprivation/reoxygenation (OGD/R)

PC12 cells were seeded onto 6-well plates in a humidified atmosphere at 37 °C with 5% CO_2. PC12 cells were pre-treated with different concentrations of Sal for 24 h before OGD. Subsequently, the culture medium was replaced with DMEM without glucose, and the cells were subjected to hypoxic conditions with 5% CO_2, 94% N_2 and 1% O_2 at 37 °C for 4 h. Then, the cells were fed normal culture medium and returned to the incubator under normoxic conditions for an additional 24 h. The viability of PC12 cells treated with different doses of Sal (1, 10 and 100 μM) was assessed by the CCK-8 assay.

Animals

Sprague-Dawley male rats (weighing 250-280 g) were obtained from Shanghai Laboratory Animal Center (Shanghai, China). All animal care and experimental procedures were approved by the Animal Research Committee of Shanghai University of Traditional Chinese Medicine and were performed according to the Guide for the Care and Use of Laboratory Animals of the National Institutes of Health Guide. All animals were housed in standard plastic cages, maintained in a temperature-controlled environment (23-25 °C) under a 12-h light/dark cycle, and allowed free access to food and water. Animals were randomly divided into six groups (n=15 for each group): sham, MCAO/R+vehicle, MCAO/R+Sal (25 mg/kg), MCAO/R+Sal (50 mg/kg), MCAO/R+Sal (100 mg/kg) and MCAO/R+H-89.

MCAO model, drug injection, and evaluation of neurological deficits

Rats were anesthetised with 2% sodium pentobarbital (30 mg/kg, i.p.). Briefly, the common carotid artery (CCA) and external carotid artery (ECA) were exposed through a ventral cervical midline incision. Microvascular clips were temporarily placed on the CCA and internal carotid artery (ICA). A fine silicon-coated surgical nylon monofilament thread (0.36 ± 0.02 mm; L3600, Jia Ling Biotechnology Co. Ltd., Guangzhou, China) was inserted from the CCA bifurcation along the ICA at approximately 18 mm to block the origin of the left MCA. Reperfusion was initiated by gently withdrawing the nylon monofilament thread after 2 h of occlusion. Rats in the sham group were operated on in the same manner except that the surgical nylon monofilament thread. Saline or different concentrations of drugs were immediately injected at the beginning of ischemia (0 h) and after reperfusion (1 h) and then once per day for seven consecutive days. The dosages of H-89 used in this study were based on those in previously published studies [51, 52].

The neurological deficits of animals were evaluated on day 7 after MCAO. Neurological function was determined using a 4-point evaluation as described previously [53]: 0 = no observable neurological deficit; 1 = failure to fully extend the right forepaw; 2 = circling to the right; 3 = failing to the right side; and 4 = no spontaneous ambulation and/or complete immobility.

Cerebral infarct assessment

Rat brains were quickly removed and coronally sectioned to a thickness of 2 mm. Subsequently, the sections were quickly immersed in a solution containing 2% TTC at 37°C in the dark for 20 min and fixed in fresh 4% paraformaldehyde in phosphate-buffered saline (PBS) for at least 1 h.

Tissue preparation and HE, Nissl, and TUNEL staining

On day 7, under deep anaesthesia with 2% sodium pentobarbital, rats were perfused through the ascending aorta with 200 ml of saline (0.9% NaCl), followed by 250 ml of ice cold fresh 4% paraformaldehyde in 0.1 M PBS (pH 7.4). After the brains containing the ischemic penumbra were fixed, paraffin and serial sections (5 μm thick) were mounted on slides coated with poly-L-lysine for HE, Nissl, TUNEL staining and immunofluorescence analyses. For histological staining, sections were stained with haematoxylin and eosin for HE staining and cresyl violet for Nissl staining, respectively. Apoptosis was assessed histologically and with an in situ cell death detection kit, according to the manufacturer's instructions. An Olympus microscope was used to collect images.

Immunofluorescence

Prepared sections were deparaffinized with xylene (changed twice, 10 min each) and rehydrated in a graded ethanol series. After rinsing in PBS three times, the sections were treated with 0.01 M sodium citrate buffer at 95 °C for 20 min for antigen retrieval, followed by incubation with 3% H_2O_2 for 10 min. Slices were blocked in 10% normal goat serum with 0.3% Triton-X-100 in 0.01 M PBS at room temperature for 1 h. Then, the slides were incubated with the primary antibody (FGF2, 1:200; c-caspase 3, 1:200; PSD95, 1:200; NeuN, 1:200) overnight at 4 °C. After incubation with the primary antibody, the sections were probed at 37 °C for 30 min with the following labelled secondary antibodies: DyLight 594-labelled goat anti-mouse IgG (1:200) and fluorescein isothiocyanate (FITC)-conjugated AffiniPure goat anti-rabbit IgG (1:200). Nuclei were stained with 4,6-diamidino-2-phenylindole (DAPI) for 5 min. Immunofluorescence was examined in the ischemic penumbra region of the cerebral cortex.

Western blot analysis

Cell supernatants and tissues were collected for protein assays. The extracted proteins were first quantified by the BCA protein assay. Cellular samples containing 30 μg of protein and tissue samples containing 80 μg of protein were separated on SDS/PAGE gels and transferred onto PVDF membranes. Then, the membranes were blocked for 1 h at room temperature (RT) with 5% skim milk and incubated with the appropriate primary antibodies at 4°C overnight. The concentrations of the primary antibodies were as follows: cAMP (1:1000), PKA(1:500), CREB (1:500), p-CREB (1:500), FGF2 (1:500), FGFR1 (1:500), TNF-α (1:500), IL-1β (1:500), IL-6 (1:500), Bax (1:500), Bcl-2 (1:500), c-caspase 3 (1:500), PSD95 (1:300), synaptotagmin (1:500), synapsin I (1:1000) and GAPDH (1:1000). The membranes were rinsed three times with TBST and incubated with horseradish peroxidase-conjugated secondary antibodies at room temperature for 2 h. The protein bands were visualized using an enhanced chemiluminescence (ECL) system (Beyotime Corp, China). Quantitative densitometric analysis was performed using AlphaEaseFC (version 4.0).

Quantitative real-time PCR

Total RNA was extracted from cultured cells and tissue samples using TRIzol reagent (Invitrogen, USA), and 1 μg of total RNA from each sample was used to synthesize cDNA (A3500, Promega). Real-time PCR amplification was performed on a Light Cycler480 system (Roche, USA) using SYBR Green (QPK-212, Tokyo, Japan). The cycling conditions were as follows: 95 °C for 5 min, followed by 40 cycles of 95 °C for 10 sec, 60 °C for 10 sec, and 72 °C for 10 sec; each sample was tested in triplicate. Tubulin was selected as an internal reference, and the gene expression levels were calculated using the $2^{-\Delta\Delta Ct}$ method. The primers for PKA, p-CREB, FGF2, FGR1, TNF-α, IL-1β, IL-6, c-caspase 3, Bcl-2, Bax and PSD95 are listed in Table 1.

Transmission electron microscopy

Tissue samples were obtained from the ischemic stroke penumbra region without heart perfusion and kept in a solution containing 2.5 % glutaraldehyde overnight. After washing in PBS three times, the samples were fixed in 1% osmic acid for 1 h and stained with 1% uranyl acetate for 2 h. After routine gradient dehydration with an acetone solution, tissues were embedded for coronal sections. Toluidine blue-stained semithin sectioning were prepared to determine the localization of neurons, and ultrathin sections were then

Table 1. Primers used for real-time PCR analysis.

Genes	Forward primers	Reverse primers
PKA	GGACAAGCAGAAGGTGGTGAAGC	ACCAGGCACGTACTCCATGACC
p-CREB	TGTTGTTCAAGCTGCCTCTGGTG	GCTTCTTCAGCAGGCTGTGTAGG
FGF2	GGTGGAAGGCTGGTCGTTGTG	TCCAGGAGACTGCCGTGACG
FGFR1	CTCTGCATGGTTGACCGTTCTGG	GCTCTTCTTGGTGCCGCTCTTC
TNF-α	GCATGATCCGAGATGTGGAACTGG	CGCCACGAGCAGGAATGAGAAG
IL-1β	ATCTCACAGCAGCATCTCGACAAG	CACACTAGCAGGTCGTCATCATCC
IL-6	AGGAGTGGCTAAGGACCAAGACC	TGCCGAGTAGACCTCATAGTGACC
C-caspase 3	GTACAGAGCTGGACTGCGGTATTG	AGTCGGCCTCCACTGGTATCTTC
Bcl-2	ACGGTGGTGGAGGAACTCTTCAG	GGTGTGCAGATGCCGGTTCAG
Bax	CCAGGACGCATCCACCAAGAAG	GCTGCCACACGGAAGAAGACC
PSD95	TCCAGTCTGTGCGAGAGGTAGC	GGACGGATGAAGATGGCGATGG
Tubulin	ATGCCAACCTTGAAGCCAGTG	GCTTTGAGCCAGCCAACCAGA

cut and imaged using a Hitachi transmission electron microscope (TEM, Hitachi, Tokyo, Japan).

Golgi staining

Golgi-Cox staining was performed using the FD Rapid Golgi Stain Kit. Fresh ischemic penumbra tissues were immersed in mixtures of equal parts of kit Solutions A and B and stored at RT for 2 weeks in the dark. Brain tissues were then transferred to solution C and kept at 4 °C for at least 48 h. All procedures were conducted in the dark. Samples were sliced into coronal sections with a thickness of 150 μm and stained according to the manufacturer's instructions.

Sholl analysis

The morphology of dendritic complexity and the spine density were assessed using Sholl analysis. The number of intersections between apical and basal dendrites in 20 μm concentric circles around the centre of the cell soma was counted. Sholl analysis was used to assess the radial distribution of dendritic material and was conducted using the Sholl analysis plug-in (available at http://fji.sc/Sholl Analysis) for ImageJ software (National Institutes of Health, Bethesda, MD, USA) to assess the number of bifurcations, the number of intersections, and the total length of the dendritic material contained in concentric circles.

Measurement of spine density

The neuronal dendritic spine density was analysed within ischemic penumbra tissues. Layer V pyramidal cells were observed at 400× magnification, a length of dendrite was traced and the number of spines along the length was counted (to yield spines/10 μm), and no attempt was made to correct for hidden spines by overlying dendrites.

Statistical analysis

SPSS 16.0 software was used for statistical analyses. Significant differences were analysed using one-way analysis of variance (ANOVA) followed by Dunnett's test ($^{\#}P < 0.05$, $^{\#\#}P < 0.01$; $^{*}P < 0.05$, $^{**}P < 0.01$). All experimental data are presented as the mean ± standard deviation (SD), and $P < 0.05$ was considered to represent a statistically significant difference.

CONFLICTS OF INTEREST

The authors declare that they have no conflicts of interest.

FUNDING

REFERENCES

1. Jia JM, Chowdary PD, Gao X, Ci B, Li W, Mulgaonkar A, Plautz EJ, Hassan G, Kumar A, Stowe AM, Yang SH, Zhou W, Sun X, et al. Control of cerebral ischemia with magnetic nanoparticles. Nat Methods. 2017; 14:160–66.
https://doi.org/10.1038/nmeth.4105
PMID:27941784

2. Tu WJ, Dong X, Zhao SJ, Yang DG, Chen H. Prognostic value of plasma neuroendocrine biomarkers in patients with acute ischaemic stroke. J Neuroendocrinol. 2013; 25:771–78.
https://doi.org/10.1111/jne.12052
PMID:23701638

3. Khoshnam SE, Winlow W, Farzaneh M, Farbood Y, Moghaddam HF. Pathogenic mechanisms following ischemic stroke. Neurol Sci. 2017; 38:1167–86.

https://doi.org/10.1007/s10072-017-2938-1
PMID:28417216

4. Xin H, Katakowski M, Wang F, Qian JY, Liu XS, Ali MM, Buller B, Zhang ZG, Chopp M. MicroRNA cluster miR-17-92 cluster in exosomes enhance neuroplasticity and functional recovery after stroke in rats. Stroke. 2017; 48:747–53.
https://doi.org/10.1161/STROKEAHA.116.015204
PMID:28232590

5. Sjöström PJ, Rancz EA, Roth A, Häusser M. Dendritic excitability and synaptic plasticity. Physiol Rev. 2008; 88:769–840.
https://doi.org/10.1152/physrev.00016.2007
PMID:18391179

6. Zhu L, Wang L, Ju F, Khan A, Cheng X, Zhang S. Reversible recovery of neuronal structures depends on the degree of neuronal damage after global cerebral ischemia in mice. Exp Neurol. 2017; 289:1–8.
https://doi.org/10.1016/j.expneurol.2016.12.002
PMID:27940018

7. Astrup J, Siesjö BK, Symon L. Thresholds in cerebral ischemia - the ischemic penumbra. Stroke. 1981; 12:723–25.
https://doi.org/10.1161/01.str.12.6.723
PMID:6272455

8. Tang TY, Jiao Y, Cui Y, Zeng CH, Zhao DL, Zhang Y, Peng CY, Yin XD, Gao PY, Yang YJ, Ju SH, Teng GJ. Development and validation of a penumbra-based predictive model for thrombolysis outcome in acute ischemic stroke patients. EBioMedicine. 2018; 35:251–59.
https://doi.org/10.1016/j.ebiom.2018.07.028
PMID:30146341

9. Deuchar GA, Brennan D, Holmes WM, Shaw M, Macrae IM, Santosh C. Perfluorocarbon enhanced glasgow oxygen level dependent (GOLD) magnetic resonance metabolic imaging identifies the penumbra following acute ischemic stroke. Theranostics. 2018; 8:1706–22.
https://doi.org/10.7150/thno.21685
PMID:29556351

10. Tsai MJ, Tsai SK, Huang MC, Liou DY, Huang SL, Hsieh WH, Huang WC, Huang SS, Cheng H. Acidic FGF promotes neurite outgrowth of cortical neurons and improves neuroprotective effect in a cerebral ischemic rat model. Neuroscience. 2015; 305:238–47.
https://doi.org/10.1016/j.neuroscience.2015.07.074
PMID:26241340

11. Woodbury ME, Ikezu T. Fibroblast growth factor-2 signaling in neurogenesis and neurodegeneration. J Neuroimmune Pharmacol. 2014; 9:92–101.
https://doi.org/10.1007/s11481-013-9501-5
PMID:24057103

12. Lim W, Bae H, Bazer FW, Song G. Fibroblast growth factor 2 induces proliferation and distribution of G$_2$/M phase of bovine endometrial cells involving activation of PI3K/AKT and MAPK cell signaling and prevention of effects of ER stress. J Cell Physiol. 2018; 233:3295–305.
https://doi.org/10.1002/jcp.26173
PMID:28885691

13. Cheng J, Chen M, Zhu JX, Li CF, Zhang QP, Geng D, Liu Q, Yi LT. FGF-2 signaling activation in the hippocampus contributes to the behavioral and cellular responses to puerarin. Biochem Pharmacol. 2019; 168:91–99.
https://doi.org/10.1016/j.bcp.2019.06.025
PMID:31251937

14. Manfè V, Kochoyan A, Bock E, Berezin V. Peptides derived from specific interaction sites of the fibroblast growth factor 2-FGF receptor complexes induce receptor activation and signaling. J Neurochem. 2010; 114:74–86.
https://doi.org/10.1111/j.1471-4159.2010.06718.x
PMID:20374425

15. Thümmler K, Rom E, Zeis T, Lindner M, Brunner S, Cole JJ, Arseni D, Mücklisch S, Edgar JM, Schaeren-Wiemers N, Yayon A, Linington C. Polarizing receptor activation dissociates fibroblast growth factor 2 mediated inhibition of myelination from its neuroprotective potential. Acta Neuropathol Commun. 2019; 7:212.
https://doi.org/10.1186/s40478-019-0864-6
PMID:31856924

16. Won SJ, Xie L, Kim SH, Tang H, Wang Y, Mao X, Banwait S, Jin K. Influence of age on the response to fibroblast growth factor-2 treatment in a rat model of stroke. Brain Res. 2006; 1123:237–44.
https://doi.org/10.1016/j.brainres.2006.09.055
PMID:17064673

17. Qiang L, Yu W, Liu M, Solowska JM, Baas PW. Basic fibroblast growth factor elicits formation of interstitial axonal branches via enhanced severing of microtubules. Mol Biol Cell. 2010; 21:334–44.
https://doi.org/10.1091/mbc.e09-09-0834
PMID:19940015

18. Baum P, Vogt MA, Gass P, Unsicker K, von Bohlen und Halbach O. FGF-2 deficiency causes dysregulation of Arhgef6 and downstream targets in the cerebral cortex accompanied by altered neurite outgrowth and dendritic spine morphology. Int J Dev Neurosci. 2016; 50:55–64.
https://doi.org/10.1016/j.ijdevneu.2016.03.002
PMID:26970009

19. Li A, Guo H, Luo X, Sheng J, Yang S, Yin Y, Zhou J, Zhou J. Apomorphine-induced activation of dopamine receptors modulates FGF-2 expression in astrocytic cultures and promotes survival of dopaminergic neurons. FASEB J. 2006; 20:1263–65.

https://doi.org/10.1096/fj.05-5510fje
PMID:16636101

20. Ghiglieri V, Napolitano F, Pelosi B, Schepisi C, Migliarini S, Di Maio A, Pendolino V, Mancini M, Sciamanna G, Vitucci D, Maddaloni G, Giampà C, Errico F, et al. Rhes influences striatal cAMP/PKA-dependent signaling and synaptic plasticity in a gender-sensitive fashion. Sci Rep. 2015; 5:10933.
https://doi.org/10.1038/srep10933
PMID:26190541

21. Wang H, Xu J, Lazarovici P, Quirion R, Zheng W. cAMP response element-binding protein (CREB): a possible signaling molecule link in the pathophysiology of schizophrenia. Front Mol Neurosci. 2018; 11:255.
https://doi.org/10.3389/fnmol.2018.00255
PMID:30214393

22. Elliott T. Dynamic integrative synaptic plasticity explains the spacing effect in the transition from short- to long-term memory. Neural Comput. 2019; 31:2212–51.
https://doi.org/10.1162/neco_a_01227
PMID:31525308

23. Copf T, Kamara M, Venkatesh T. Axon length maintenance and synapse integrity are regulated by c-AMP-dependent protein kinase a (PKA) during larval growth of the drosophila sensory neurons. J Neurogenet. 2019; 33:157–63.
https://doi.org/10.1080/01677063.2019.1586896
PMID:30955404

24. Zhang H, Meng J, Li X, Zhou S, Qu D, Wang N, Jia M, Ma X, Luo X. pro-GLP-1, a pro-drug of GLP-1, is neuroprotective in cerebral ischemia. Eur J Pharm Sci. 2015; 70:82–91.
https://doi.org/10.1016/j.ejps.2015.01.010
PMID:25640912

25. Zuo L, Shi L, Yan F. The reciprocal interaction of sympathetic nervous system and cAMP-PKA-NF-kB pathway in immune suppression after experimental stroke. Neurosci Lett. 2016; 627:205–10.
https://doi.org/10.1016/j.neulet.2016.05.066
PMID:27250857

26. Wu S, Zhang W, Ma S, Li B, Xu C, Yi P. ERK1/2 and JNK signaling synergistically modulate mitogenic effect of fibroblast growth factor 2 on liver cell. Cell Biol Int. 2018; 42:1511–22.
https://doi.org/10.1002/cbin.11043
PMID:30080297

27. Cui G, Chen H, Cui W, Guo X, Fang J, Liu A, Chen Y, Lee SM. FGF2 prevents sunitinib-induced cardiotoxicity in zebrafish and cardiomyoblast H9c2 cells. Cardiovasc Toxicol. 2016; 16:46–53.
https://doi.org/10.1007/s12012-015-9315-1
PMID:25701259

28. Bu Q, Wang A, Hamzah H, Waldman A, Jiang K, Dong Q, Li R, Kim J, Turner D, Chang Q. CREB signaling is involved in rett syndrome pathogenesis. J Neurosci. 2017; 37:3671–85.
https://doi.org/10.1523/JNEUROSCI.3735-16.2017
PMID:28270572

29. Bai H, Zhao L, Liu H, Guo H, Guo W, Zheng L, Liu X, Wu X, Luo J, Li X, Gao L, Feng D, Qu Y. Adiponectin confers neuroprotection against cerebral ischemia-reperfusion injury through activating the cAMP/PKA-CREB-BDNF signaling. Brain Res Bull. 2018; 143:145–54.
https://doi.org/10.1016/j.brainresbull.2018.10.013
PMID:30395885

30. Wei Y, Hong H, Zhang X, Lai W, Wang Y, Chu K, Brown J, Hong G, Chen L. Salidroside inhibits inflammation through PI3K/akt/HIF signaling after focal cerebral ischemia in rats. Inflammation. 2017; 40:1297–309.
https://doi.org/10.1007/s10753-017-0573-x
PMID:28478514

31. Li Q, Wang J, Li Y, Xu X. Neuroprotective effects of salidroside administration in a mouse model of alzheimer's disease. Mol Med Rep. 2018; 17:7287–92.
https://doi.org/10.3892/mmr.2018.8757
PMID:29568861

32. Xu N, Huang F, Jian C, Qin L, Lu F, Wang Y, Zhang Z, Zhang Q. Neuroprotective effect of salidroside against central nervous system inflammation-induced cognitive deficits: a pivotal role of sirtuin 1-dependent nrf-2/HO-1/NF-κB pathway. Phytother Res. 2019; 33:1438–47.
https://doi.org/10.1002/ptr.6335
PMID:30848530

33. Dimpfel W, Schombert L, Panossian AG. Assessing the quality and potential efficacy of commercial extracts of Rhodiola rosea L. By analyzing the salidroside and rosavin content and the electrophysiological activity in hippocampal long-term potentiation, a synaptic model of memory. Front Pharmacol. 2018; 9:425.
https://doi.org/10.3389/fphar.2018.00425
PMID:29881348

34. Lai W, Zheng Z, Zhang X, Wei Y, Chu K, Brown J, Hong G, Chen L. Salidroside-mediated neuroprotection is associated with induction of early growth response genes (egrs) across a wide therapeutic window. Neurotox Res. 2015; 28:108–21.
https://doi.org/10.1007/s12640-015-9529-9
PMID:25911293

35. Jin R, Liu L, Zhang S, Nanda A, Li G. Role of inflammation and its mediators in acute ischemic stroke. J Cardiovasc Transl Res. 2013; 6:834–51.
https://doi.org/10.1007/s12265-013-9508-6
PMID:24006091

36. Tuttolomondo A, Maida C, Pinto A. Inflammation and Inflammatory Cell Recruitment in Acute Cerebrovascular Diseases. Current Immunology Reviews. 2015; 11:24–32.
https://doi.org/10.2174/1573395511101150417101550

37. Ahmad M, Graham SH. Inflammation after stroke: mechanisms and therapeutic approaches. Transl Stroke Res. 2010; 1:74–84.
https://doi.org/10.1007/s12975-010-0023-7
PMID:20976117

38. Brough D, Rothwell NJ. Caspase-1-dependent processing of pro-interleukin-1beta is cytosolic and precedes cell death. J Cell Sci. 2007; 120:772–81.
https://doi.org/10.1242/jcs.03377 PMID:17284521

39. Suzuki S, Tanaka K, Suzuki N. Ambivalent aspects of interleukin-6 in cerebral ischemia: inflammatory versus neurotrophic aspects. J Cereb Blood Flow Metab. 2009; 29:464–79.
https://doi.org/10.1038/jcbfm.2008.141
PMID:19018268

40. Gipson CD, Olive MF. Structural and functional plasticity of dendritic spines - root or result of behavior? Genes Brain Behav. 2017; 16:101–17.
https://doi.org/10.1111/gbb.12324 PMID:27561549

41. Brown CE, Murphy TH. Livin' on the edge: imaging dendritic spine turnover in the peri-infarct zone during ischemic stroke and recovery. Neuroscientist. 2008; 14:139–46.
https://doi.org/10.1177/1073858407309854
PMID:18039977

42. McLeod DD, Parsons MW, Hood R, Hiles B, Allen J, McCann SK, Murtha L, Calford MB, Levi CR, Spratt NJ. Perfusion computed tomography thresholds defining ischemic penumbra and infarct core: studies in a rat stroke model. Int J Stroke. 2015; 10:553–59.
https://doi.org/10.1111/ijs.12147 PMID:24138577

43. Brown CE, Wong C, Murphy TH. Rapid morphologic plasticity of peri-infarct dendritic spines after focal ischemic stroke. Stroke. 2008; 39:1286–91.
https://doi.org/10.1161/STROKEAHA.107.498238
PMID:18323506

44. Liu M, Wu Y, Liu Y, Chen Z, He S, Zhang H, Wu L, Tu F, Zhao Y, Liu C, Chen X. Basic fibroblast growth factor protects astrocytes against ischemia/reperfusion injury by upregulating the caveolin-1/VEGF signaling pathway. J Mol Neurosci. 2018; 64:211–23.
https://doi.org/10.1007/s12031-017-1023-9
PMID:29299743

45. Pang Q, Zhang H, Chen Z, Wu Y, Bai M, Liu Y, Zhao Y, Tu F, Liu C, Chen X. Role of caveolin-1/vascular endothelial growth factor pathway in basic fibroblast growth factor-induced angiogenesis and neurogenesis after treadmill training following focal cerebral ischemia in rats. Brain Res. 2017; 1663:9–19.
https://doi.org/10.1016/j.brainres.2017.03.012
PMID:28300551

46. Wang YL, Zhu XL, Sun MH, Dang YK. Effects of astaxanthin onaxonal regeneration via cAMP/PKA signaling pathway in mice with focal cerebral infarction. Eur Rev Med Pharmacol Sci. 2019; 23:135–43.
https://doi.org/10.26355/eurrev_201908_18640
PMID:31389584

47. Gao X, Zhang X, Cui L, Chen R, Zhang C, Xue J, Zhang L, He W, Li J, Wei S, Wei M, Cui H. Ginsenoside Rb1 promotes motor functional recovery and axonal regeneration in post-stroke mice through cAMP/PKA/CREB signaling pathway. Brain Res Bull. 2020; 154:51–60.
https://doi.org/10.1016/j.brainresbull.2019.10.006
PMID:31715311

48. Stein A, Radhakrishnan A, Riedel D, Fasshauer D, Jahn R. Synaptotagmin activates membrane fusion through a Ca2+-dependent trans interaction with phospholipids. Nat Struct Mol Biol. 2007; 14:904–11.
https://doi.org/10.1038/nsmb1305 PMID:17891149

49. Brenes O, Giachello CN, Corradi AM, Ghirardi M, Montarolo PG. Synapsin knockdown is associated with decreased neurite outgrowth, functional synaptogenesis impairment, and fast high-frequency neurotransmitter release. J Neurosci Res. 2015; 93:1492–506.
https://doi.org/10.1002/jnr.23624 PMID:26213348

50. Vickers CA, Stephens B, Bowen J, Arbuthnott GW, Grant SG, Ingham CA. Neurone specific regulation of dendritic spines in vivo by post synaptic density 95 protein (PSD-95). Brain Res. 2006; 1090:89–98.
https://doi.org/10.1016/j.brainres.2006.03.075
PMID:16677619

51. Xia Y, Zhan C, Feng M, Leblanc M, Ke E, Yeddula N, Verma IM. Targeting CREB pathway suppresses small cell lung cancer. Mol Cancer Res. 2018; 16:825–32.
https://doi.org/10.1158/1541-7786.MCR-17-0576
PMID:29523765

52. Wang MD, Huang Y, Zhang GP, Mao L, Xia YP, Mei YW, Hu B. Exendin-4 improved rat cortical neuron survival under oxygen/glucose deprivation through PKA pathway. Neuroscience. 2012; 226:388–96.
https://doi.org/10.1016/j.neuroscience.2012.09.025
PMID:23000625

53. Longa EZ, Weinstein PR, Carlson S, Cummins R. Reversible middle cerebral artery occlusion without craniectomy in rats. Stroke. 1989; 20:84–91.
https://doi.org/10.1161/01.str.20.1.84
PMID:2643202